Determining the in-plane Fermi surface topology in high T_c superconductors using angle-dependent magnetic quantum oscillations

FAST TRACK COMMUNICATION

Determining the in-plane Fermi surface topology in high T_c superconductors using angle-dependent magnetic quantum oscillations

N Harrison and R D McDonald

National High Magnetic Field Laboratory, Los Alamos National Laboratory, MS E536,
Los Alamos, NM 87545, USA

Abstract

We propose a quantum oscillation experiment by which the rotation of an underdoped $YBa_2Cu_3O_{6+x}$ sample about two different axes with respect to the orientation of the magnetic field can be used to infer the shape of the in-plane cross-section of corrugated Fermi surface cylinder(s). Deep corrugations in the Fermi surface are expected to give rise to nodes in the quantum oscillation amplitude that depend on the magnitude and orientation of the magnetic induction **B**. Because the symmetries of electron and hole cylinders within the Brillouin zone are expected to be very different, the topology can provide essential clues as to the broken symmetry responsible for the observed oscillations. The criterion for the applicability of this method to the cuprate superconductors (as well as other layered metals) is that the difference in quantum oscillation frequency $2\Delta F$ between the maximum (belly) and minimum (neck) extremal cross-sections of the corrugated Fermi surface exceeds $|\mathbf{B}|$.

(Some figures in this article are in colour only in the electronic version)

The recent discovery of magnetic quantum oscillations in high temperature superconductors provides an entirely new perspective on their electronic structure [1–5]. These experiments provide evidence for a Fermi surface and possible evidence for a broken symmetry groundstate in underdoped samples, yet the precise form of the symmetry remains the subject of debate. A key point of discussion is the carrier sign of the pocket responsible for the largest amplitude quantum oscillations in $YBa_2Cu_3O_{6+x}$ and $YBa_2Cu_4O_8$ [1, 6]. Quantum oscillation experiments cannot directly infer the sign of the carriers, leaving open many possibilities for the interpretation of the negative Hall coefficient and topology of the Fermi surface [7–13]. The choice between electron and hole pockets cannot be taken lightly. If the carriers are truly electron-like then this places limitations on the types of theoretical model that can be applied to the underdoped metallic state of high T_c superconductors. Given the possible implications for the competing order parameters in $YBa_2Cu_3O_{6+x}$, a thorough

experimental investigation of the Fermi surface topology is of paramount importance.

In this paper we show that crucial clues as to the nature of the broken symmetry phase that competes with superconductivity may be found by performing quantum oscillation experiments in which the crystalline c axis of the sample is tilted away from axis of the magnetic induction **B** in different directions. The recently proposed deeply corrugated form of the Fermi surface cylinder(s) [14, 15] implies the existence of beats in the quantum oscillation amplitude as a function of the magnitude and orientation of **B**. By tracking the position of nodes in the quantum oscillation amplitude, the shape of the in-plane cross-section of the cylinders can be mapped out in a similar fashion to angle-dependent magnetoresistance oscillations (AMRO) [16]. A distinction between electron and hole pockets can be made because they are predicted to have different symmetry properties within the Brillouin zone (as depicted for the simple case of $\mathbf{Q} = (\pi, \pi)$
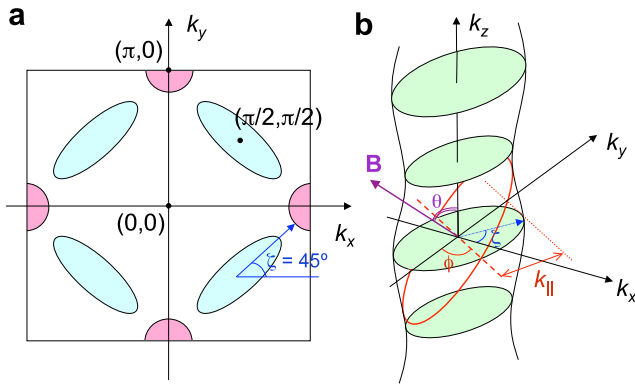
1

Figure 1. (a) Schematic Fermi surface for the simple case of
$\mathbf{Q} = (\pi, \pi)$ density wave ordering, leading to reconstructed electron
(pink) and highly elliptical hole (cyan) pockets. The electron pockets
are expected to vanish in strong-coupling models. (b) Schematic
warped Fermi surface with an elliptical cross-section with its major
axis at an arbitrary orientation ζ within the k_x, k_y plane. The
extremal cross-sections orthogonal to k_z and $\mathbf{c}$ are depicted in green.
The red curve shows an example orbit when the magnetic induction
$\mathbf{B}$ is rotated by a 'zenithal' angle θ away from the k_z axis. The half
caliper width of the in-plane cross-section $k_\parallel$ depends on the
'azimuthal' component ϕ of the magnetic field orientation and on ζ.

ordering in figure 1(a)), the details of which may further
depend on the precise form of the broken symmetry.

Independent of the broken symmetry responsible for the
creation of a given corrugated Fermi surface cylinder, the k_z-
dependence of the cross-sectional area A_k can be expanded as a
series of harmonics. A schematic of a corrugated Fermi surface
cylinder is shown in figure 1(b). If the in-plane crystal lattice
vectors $\mathbf{a}$ and $\mathbf{b}$ are orthogonal to the interlayer vector $\mathbf{c}$, A_k
can be considered as the sum of even harmonics

$$A_k = \sum_n A_n \cos(nk_z c) \quad (1)$$

where $c = |\mathbf{c}|$. Here, A_0 is the mean cross-sectional area of
the Fermi surface, $A_{n \geqslant 1} \approx 4\pi m^* t_{c,n}/\hbar^2$ represent harmonics
of the corrugation and m^* is the in-plane effective mass. In
the presence of a magnetic induction $\mathbf{B}$, the k-space area $A_{\theta,\phi}$
of a given semiclassical orbit (depicted in red in figure 1(b))
depends on the 'zenithal' θ and 'azimuthal' ϕ orientation
of $\mathbf{B}$ with respect to the corrugated cylinder (as depicted in
figure 1(b)). The orbit area in such a situation was found by
Yamaji [17] to have the form

$$A_{\theta,\phi} \cos\theta = \sum_n A_n J_0(nk_\parallel c \tan\theta) \cos(nk_{z,0} c). \quad (2)$$

Its further dependence on the half caliper width $k_\parallel$ of the
corrugated cylinder within the k_x, k_y plane was considered
in subsequent works [16]. Here $J_0(x)$ is the zeroth order
Bessel function, while $k_{z,0}$ is the k_z coordinate of the geometric
center of the orbit. If the in-plane cross-section is elliptical in
form, as if often approximately the case for small pockets of
carriers [16], then

$$k_\parallel = k_F \sqrt{\eta \cos^2(\phi - \zeta) + \frac{1}{\eta} \sin^2(\phi - \zeta)}, \quad (3)$$

where $k_F = \sqrt{A_0/\pi}$ is the effective Fermi radius, η is the
ellipticity of the pocket (or the ratio between major and minor
axes) and ζ is the orientation of its major axis with respect
to k_x within the k_x, k_y plane. For $\eta = 1$, this reduces to a
perfect circle where $k_\parallel = k_F$, as was originally considered by
Yamaji [17]. The $k_{z,0}$-dependence of the quantum oscillation
frequency is obtained applying Onsager's relation

$$F_{\theta,\phi} = \left(\frac{\hbar}{2\pi e}\right) A_{\theta,\phi} \quad (4)$$

to equation (2). Finally, the form of the magnetic quantum
oscillations is obtained by integrating over $k_{z,0}$. On neglecting
oscillations of the chemical potential (assuming that the
corrugation is large), the oscillatory magnetization is given
by [18]

$$M_z = -\frac{1}{\pi} \int_{-\pi/c}^{\pi/c} \sum_{\zeta,p,n} M_p \sin\left(2\pi p\left(\frac{F_{\theta,\phi}}{B} - \frac{1}{2}\right)\right) dk_{z,0} \quad (5)$$

where

$$M_p = \left(\frac{\hbar e N}{pm^*}\right) \frac{X_p}{\sinh X_p} \exp\left(-\frac{p\Gamma}{B}\right) \cos\left(\frac{\pi p m^* g}{m_e \cos\theta}\right) \quad (6)$$

are the conventional amplitude-modifying prefactors and
$X_p = 2\pi^2 pm^* k_B T/\hbar eB$ [18]. Here, p is the quantum
oscillation harmonic index. The term containing the hyperbolic
sine is the thermal damping factor, the exponential factor
accounts for quasiparticle scattering, while the cosine term
accounts for Zeeman splitting (or 'spin splitting') [18].

To understand the basic form of the $\mathbf{B}$-dependent quantum
oscillation amplitude, it is instructive to first consider the
simpler situation in which the second harmonic of the
corrugation $A_{n \geqslant 2}$ is neglected (along with higher harmonics).
In this case, the integral given by equation (5) has the simple
solution

$$M_z \approx -\frac{1}{\pi} \sum_{\zeta,p} M_p J_0\left(\frac{2\pi p \Delta F_{\theta,\phi}}{B}\right) \sin\left(2\pi p\left(\frac{F_0}{B} - \frac{1}{2}\right)\right), \quad (7)$$

where $\Delta F_{\theta,\phi} = \Delta F J_0(k_\parallel c \tan\theta)/\cos\theta$ is the difference
in frequency between maxima ('belly') and minima ('neck')
frequencies of the corrugated cylinder (with ΔF being that at
$\theta = 0$). In AMRO experiments, one is typically concerned
with the 'magic' angles at which $\Delta F_{\theta,\phi}$ vanishes [16, 17]—
where the electronic structure mimics that of an ideal two-
dimensional metal. However, nodes in the quantum oscillation
amplitude, which occur for a finite value of $\Delta F_{\theta,\phi}$, can
be determined with greater accuracy in quantum oscillation
experiments. Since $\Delta F_{\theta,\phi} > B/8\pi$ in the limit where we
consider nodes, equation (7) can be accurately approximated
by the superposition

$$M_z \approx -\frac{1}{\pi^2} \sum_{\zeta,p} M_p \sqrt{\frac{B}{p \Delta F_{\theta,\phi}}}$$
$$\times \sin\left(2\pi p\left(\frac{F_0 \mp \Delta F_{\theta,\phi}}{B} - \frac{1}{2}\right) \pm \frac{\pi}{4}\right) \quad (8)$$
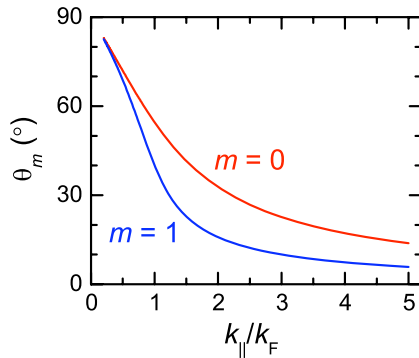
Figure 2. A plot of $\cot\theta_m$ versus $k_\parallel/k_F$ according to equation (9) for $m = 0$ and 1, using $c = 11.68$ Å and $\Delta F/B = 1$ (approximately applicable to YBa$_2$Cu$_3$O$_{6.54}$ at $B = 40$ T). For simplicity, we consider only the nodes occurring when $k_\parallel c \tan\theta_m < \frac{3\pi}{4}$.

Figure 3. Simulation of the magnetization (or magnetic torque $\tau \propto -M_z B$) from [14] using equation (5) and four adjustable parameters $F_0 = (\hbar/2\pi e)A_0 \approx 513$ T, $\Delta F = (\hbar/2\pi e)A_1 \approx 40$ T and $\Delta F_2 = (\hbar/2\pi e)A_2 \approx -10$ T in equation (1) and $\Gamma = 170$ T in equation (6). These values yield $F_{\text{neck}} \approx 463$ T and $F_{\text{belly}} \approx 543$ T. We have assumed the phase to be a fixed quantity in equation (5) (see footnote 1). We have also assumed $T = 1$ K, $m^*/m_e = 1.7$ and $g = 0$ to be fixed quantities, although inaccuracies in T or m^* are easily compensated by an adjustment of Γ and thus have little affect on the waveform.

of neck $F_{\text{neck}} = F_0 - \Delta F_{\theta,\phi}$ and belly $F_{\text{belly}} = F_0 + \Delta F_{\theta,\phi}$ quantum oscillations, giving rise to a distinctive beat pattern. Nodes occur whenever the F_{neck} and F_{belly} oscillations are π out of phase, which occurs at a different set of 'magic' angles θ_m given by

$$J_0(k_\parallel c \tan\theta_m) = \frac{(4m+3)B}{8\Delta F}\cos\theta_m, \qquad (9)$$

where m is an integer. The monotonic dependence of the mth node θ_m on $k_\parallel/k_F$ in figure 2 (in which $m = 1$ and 0 are plotted) implies that its ϕ-dependent angular position can be used to map the shape of the cylinder cross-section.

We now turn to θ-dependent simulations of M_z in underdoped YBa$_2$Cu$_3$O$_{6+x}$ for several different Fermi surface topology scenarios. Recent quantum oscillation measurements on YBa$_2$Cu$_3$O$_{6.54}$ [14, 15] (detected over a wide interval in magnetic field $B \approx \mu_0 H$) provide estimates for the relevant parameters. With the exception of the weak 637 T frequency [14], the full waveform from [14] can be reproduced in figure 3 by numerical integration of equation (5) and the adjustment of only four parameters[1] (listed in the figure caption).

We begin by considering scenarios in which the $F \sim 500$ T frequency corresponds to an electron pocket cylinder, for which a single value of $k_\parallel$ is expected at each azimuthal angle ϕ. Several different proposals for the groundstate of YBa$_2$Cu$_3$O$_{6+x}$ predict electron pockets that are approximately circular in cross-section and situated near $\mathbf{k} = (\pi, 0)$ in figure 1(a). These include $\mathbf{Q} = (\pi, \pi)$ spin- or d-density wave ordering [4, 10], certain types of spin stripe ordering in which $\mathbf{Q} = (\pi[1 \pm 2\delta], \pi)$ where $\delta = \frac{1}{8}$ [7] and helical or spiral ordering [4, 10]. Strong-coupling treatments in which the hopping of quasiparticles is frustrated by antiferromagnetic

correlations can also predict circular electron pockets under certain conditions [11], although in this case they are situated at $\mathbf{k} = (\pi, \pi)$. In all these cases, a circular electron pocket implies that $k_\parallel \approx k_F$ for all ϕ, in which case nodes corresponding to $m = 1$ and 0 should be observed at $\theta_1 \approx 40°$ and $\theta_0 \approx 55°$ when $B = 40$ T at all values of ϕ (as shown in figure 4(a)). Figure 5(a) shows the calculated θ-dependent magnetization (using the same parameters as in figure 3). Nodes at θ_1 and θ_0 are clearly evident in the simulation made using equation (8) in which the second harmonic of the corrugation A_2 is neglected (black curve), and remain discernible and at the same positions in the simulation made using equation (5) in which A_2 is included (green curve).

Under certain conditions, the electron cross-sectional area can deviate from an ideal circular form. In $\delta = \frac{1}{8}$ stripe models that incorporate both spin and charge ordering (e.g. figures 3(c) and (d) from [7]), for example, the cross-section is expected to become elongated along k_x. In figure 4(b) this situation is approximated by an ellipsoidal pocket with $\eta = 2$ and $\zeta = 0$. The reduced symmetry of the pocket is reflected in the ϕ-dependence of the angular sweeps in figures 5(a) and (b). For $\phi = 90°$ (in which, since $\zeta = 0$, the axis of rotation corresponds to the major axis) θ_1 and θ_0 are pushed out to very high angles in figure 5(b), becoming practically unobservable for the simulation made using equation (5) in which A_2 is included. For $\phi = 0$, by contrast, θ_1 and θ_0 are reduced to small angles in figures 4(b) and 5(c). If the unreconstructed Fermi surface is more circular in form [10], spiral or d-density wave order can give rise to trapezoidal-shaped electron pocket cross-sections, as shown in figure 4(c) (using $\mathbf{Q} = (\pi[1 + 2\delta], \pi)$ where $\delta = 0.1$). In spite of the loss of rotational symmetry, the ϕ-dependent $k_\parallel$ is similar to that of an ellipse, but with its major axis along k_y. Since the ϕ dependences of θ_1 and θ_2 are rotated by 90° with respect to figure 4(b), their measurement can by used to distinguish stripe and spiral or d-density wave scenarios, or perhaps other scenarios [20].

---

[1] The ability of equation (5) to reproduce the waveform with only four parameters suggests that a uniform Γ (which is proportional to the quasiparticle scattering rate [18]) provides an adequate approximation, but that a $n = 2$ component of corrugation must be taken into consideration. The ability of equation (5) to reproduce the experimental magnetization implies that there is no Berry phase. The sign of τ (which results from a vector product in the experiment) is assumed to be negative in order to correctly account for the inferred sign of M_z from [19].
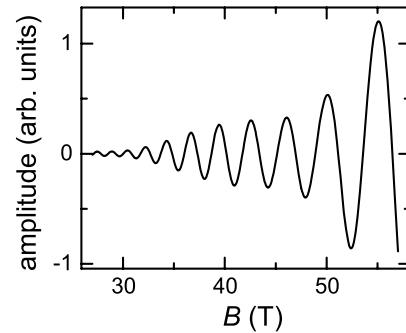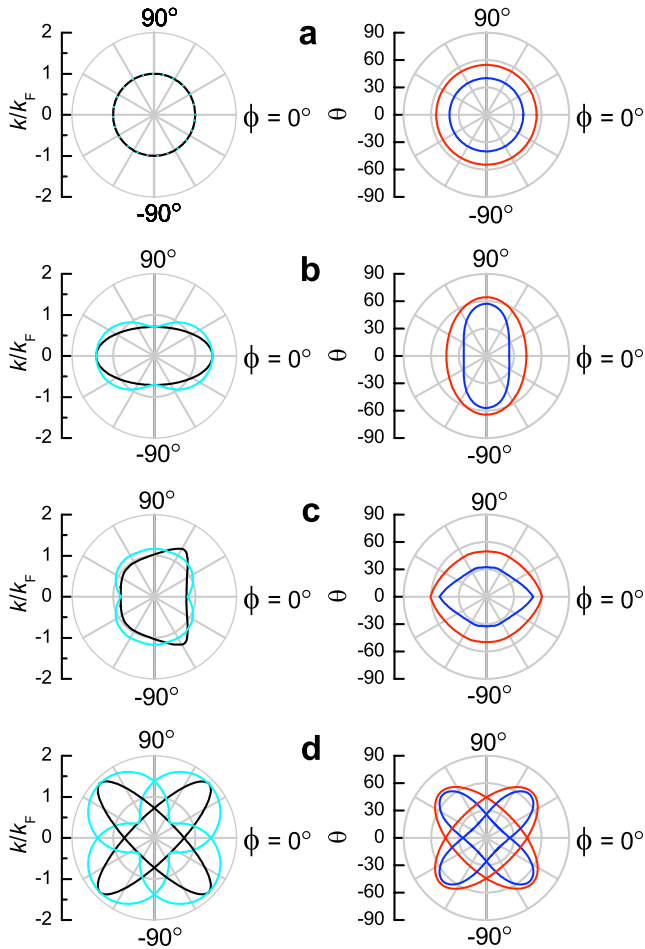
Figure 4. Polar plots (cyan) of $k_\parallel$ versus ϕ (left-hand-side) for different cylinder cross-sections (black), together with polar plots of θ_1 (blue) and θ_0 (red) versus ϕ (right-hand-side). The estimates of θ_1 and θ_0 are made at $B = 40$ T, corresponding to $\Delta F/B = 1$ in equation (9) and figure 2. Polar plot (a) corresponds to a simple circular corrugated cylinder cross-section for which $k_\parallel = k_F$, (b) corresponds an elliptical electron pocket with an ellipticity of $\eta = 2$ and orientation $\zeta = 0$ predicted in $\frac{1}{8}$th stripe models that combine spin and charge ordering, while (c) corresponds to an electron pocket of unusual cross-section predicted by certain d-density wave or spiral ordering models. (d) corresponds to highly elliptic hole pockets ($\eta = 3.5$) for which two different orientations $\zeta \approx \pm 45°$ within the k_x, k_y plane are expected, giving rise to two different values of $k_\parallel$ for each value of ϕ.

Turning now to the case where the $F \sim 500$ T frequency originates from hole pockets [1, 9, 12], the ϕ-dependences of $k_\parallel$, θ_1 and θ_0 in figure 4(d) and the forms of the θ-dependent curves in figures 5(d)–(f) become very different from those of electron pockets. In the hole pocket simulations we have assumed $\eta = 3.5$, which is approximately what might be expected were the Fermi surface obtained in recent angle-resolved photoemission experiments [9] folded about the $(\pi, 0) - (0, \pi)$ line. Since there are two different orientations $\zeta \approx \pm 45°$ to be counted in figure 4(d) and equation (5), two different values of $k_\parallel$ give rise to four simultaneously beating frequencies, leading to more complicated θ-dependent curves in figures 5(d)–(f). On the other hand, the θ-dependent curves exhibit a distinctive fourfold symmetry that changes rapidly with ϕ owing to the highly elliptical cross-sections of the
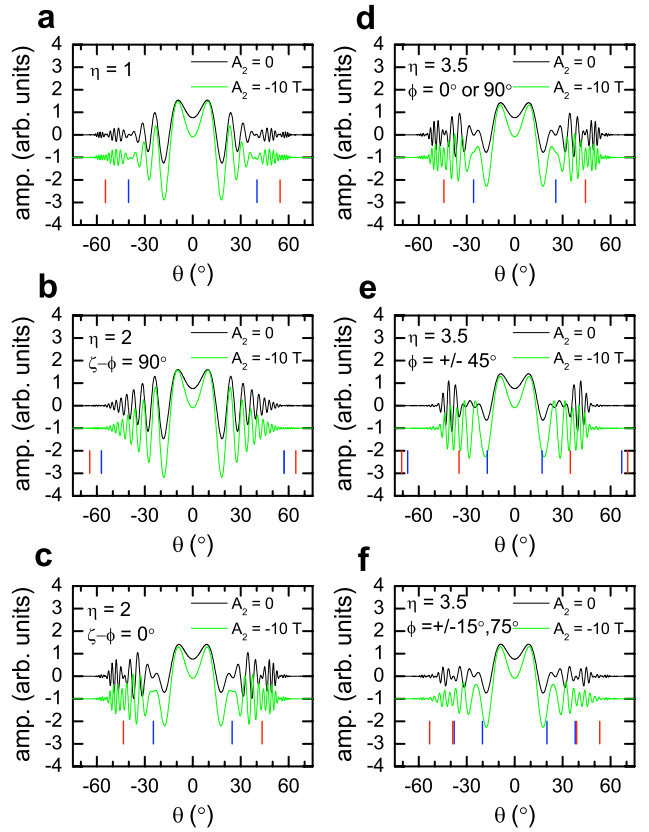

Figure 5. Examples of θ-dependent simulations at $B = 40$ T made using equation (5) using the parameters listed in figure 3 caption (green curves) and using equation (7) in which A_2 is neglected (black curves) for several different scenarios depicted in figure 4. Curve (a) is the expected θ-dependence for a simple circular cross-section, while (b) and (c) are the expected curves obtained on rotating about the major and minor axes (respectively) of the elliptical pocket with $\eta = 2$ shown in figure 4(b). (d)–(f) are examples of the θ-dependence expected for the highly elliptical hole pockets in figure 4(d) in which there are two different values of $k_\parallel$ for each value of ϕ (with the exception of $\phi = 0°$ or 90° (d) where they become degenerate). The red and blue vertical lines point to the locations of θ_0 and θ_1 respectively.

pockets. For most arbitrary values of ϕ (e.g. figure 5(e)), the contribution from two very different values of $k_\parallel$ make the nodes somewhat difficult to locate. Distinct nodes do appear, however, at $\phi = 0$ and 90° in figure 5(d) when the two values of $k_\parallel$ become degenerate, or near $\phi \approx \pm 15°$ and $\pm 75°$ in figure 5(f) due to a serendipitous degeneracy of θ_1 and θ_0. For this reason, rather detailed ϕ-dependent measurements are required to pin down the precise geometry of the cross-section of hole pockets.

In summary, we have shown that nodes in the quantum oscillation amplitude detected in dual axis rotation experiments can be used to infer the cross-sectional shape of corrugated Fermi surface cylinders in underdoped YBa$_2$Cu$_3$O$_{6+x}$, which can help to answer the question as to whether the prominent ~ 500 T frequency originates from electron- or hole-like carriers, as well as providing essential clues for the groundstate description. An advantage of this proposed method over AMRO experiments [16, 17] is that the shape of the cross-

section is linked directly to the pocket responsible for the quantum oscillations (which needs always to be assumed in AMRO experimenta). A further advantage is that the predicted nodes occur at small values of θ where H_{c2} is lower, thereby proving less of an obstacle for Fermi surface measurements.

There are, however, potential caveats. In the present simulations we have assumed that the corrugation of the Fermi cylinders is caused by simple interlayer hopping terms $t_{c,n}$. More complicated forms of warping that vary with k_x and k_y may lead to some degree of variation from the present simulations. A k_z-dependent damping factor, meanwhile (for which there is presently no evidence (see footnote 1)), will diminish the presence of nodes, while Zeeman splitting effects (presently neglected by setting $g = 0$ [15]) will lead to additional nodes unrelated to the corrugation. Nodes due to Zeeman splitting (often called 'spin splitting zeroes') typically depend only on θ, in contrast to those caused by corrugation described here, which depend on B, ϕ and θ.

References

[1] Doiron-Leyraud N *et al* 2007 *Nature* **447** 565
[2] Yelland E A *et al* 2008 *Phys. Rev. Lett.* **100** 047003
[3] Bangura A F *et al* 2008 *Phys. Rev. Lett.* **100** 046004
[4] Sebastian S E *et al* 2008 *Nature* **454** 200
[5] Vignolle B *et al* 2008 *Nature* **455** 952
[6] LeBoeuf D *et al* 2007 *Nature* **450** 533
[7] Millis A J and Norman M R 2007 *Phys. Rev. B* **76** 220503
[8] Chen W-Q *et al* 2008 *Europhys. Lett.* **82** 17004
[9] Hossain M A *et al* 2008 *Nat. Phys.* **4** 527
[10] Dimov I *et al* 2008 *Phys. Rev. B* **78** 134529
[11] Hozoi L, Laad M S and Fulde P 2008 *Phys. Rev. B* **78** 165107
[12] Chen K-T and Lee P A 2008 arXiv:0812.3351
     Lee P A 2007 arXiv:0708.2115
[13] Varma C M 2009 *Phys. Rev. B* **79** 085110
[14] Audouard A *et al* 2008 arXiv:0812.0458
[15] Sebastian S E 2008 unpublished
[16] Nam M-S *et al* 2001 *J. Phys.: Condens. Matter* **13** 2271
[17] Yamaji K 1989 *J. Phys. Soc. Japan* **58** 1520
[18] Shoeberg D 1984 *Magnetic Oscillations in Metals*
     (Cambridge: Cambridge University Press)
[19] Jaudet C *et al* 2008 arXiv:0711.3559
[20] Harrison N 2009 arXiv:0902.2741